Plasma Deposition and Etching of Diamond-Like Carbon Films

Moses David, Raghunath Padiyath, and Suryadevara V. Babu
Center for Advanced Materials Processing, Dept. of Chemical Engineering, Clarkson University, Potsdam, NY 13676

Diamond-like carbon films have been deposited from ternary mixtures of butadiene, hydrogen and argon in a parallel plate plasma reactor at constant pressure and power. These films have been etched in O_2 and CF_4/O_2 plasma discharges. A new linear relationship between the composition of the deposition gas mixture and a dimensionless number (E_N) defined in terms of etch and deposition rates and the bias voltage during deposition has been derived. E_N is a function of the ion flux during deposition. Electron-impact ionization processes are considered for relating the ion flux to the feed gas composition and ionization potentials. The etch and deposition rate data follow this linear relationship very well. The proportionality constant in this linear relationship varies with composition for CF_4/O_2 etching data. Film hardness and failure modes on silicon and glass substrates are also described.

Introduction

Plasma-deposited carbon thin films have been receiving increasing attention due to their excellent mechanical, chemical, electrical, optical and acoustic properties. Their properties can be fine-tuned for specific applications by choosing the appropriate deposition conditions. Thus, carbon films can be deposited in the form of graphite, diamond, diamond-like carbon, (DLC), diamond-like hydrocarbon and amorphous carbon. Diamond and graphite are the crystalline allotropes of carbon. The isotropic, tetrahedrally-coordinated structure of diamond and the layered, two-dimensional structure of graphite represent the two structural extremes of carbon. Amorphous carbon is yet another allotrope of carbon, whose structure is isotropic. The bonding microstructure of amorphous carbon has been of intense interest and speculated for more than a decade. The details of the microstructure are still open questions.

Plasma-deposited amorphous carbon films may contain significant amounts of hydrogen and, in that respect, are analogous to amorphous, hydrogenated silicon films. Unlike silicon, however, carbon readily forms double and triple bonds. Therefore, the possible bonding structures for carbon are far more complex than those for silicon. Both tetrahedrally-coordinated sp^3 structures and trigonally-bonded sp^2 structures exist in plasma-deposited carbon films and the film properties are correlated strongly to the relative occurrence of these configurations as well as the chemical composition. These bonding structures may involve both carbon and hydrogen atoms. Diamond films contain carbon sp^3 structures, while graphite films are predominantly sp^2 structures. The term *diamond-like carbon* is applied to the films with a significant amount of tetrahedral bonding. A more precise definition has been proposed (Angus et al., 1986) for characterizing these carbon films based on the gram-atom number density ρ_N and the term *diamond-like* has been applied to films having $\rho_N > 0.2$ g·atom/cm^3.

The earliest carbon films were deposited from carbon ions extracted from a carbon arc in argon (Aisenberg and Chabot, 1971). Spencer et al. (1976), Holland and Ojha (1976, 1978, 1979), Ojha and Holland (1977), Weissmantel (1979, 1982), Wada et al. (1980), Bubenzer et al. (1983), Vora and Moravec (1981), and Angus et al. (1968, 1984) were among the most active early workers. Their work led to an almost explosive growth of the field, which has been reviewed thoroughly in the last few years (Angus et al., 1986, 1988, 1989; Phillips, 1979; Martin et al., 1989; Tsai and Bogy, 1987; Messier et al., 1987; Bachmann and Messier, 1989).

Several techniques were used for depositing carbon films, using both solid carbon and hydrocarbon sources. Sputtering, laser evaporation, pulsed discharge rail gun, and cathodic arc deposition employed solid carbon, while ion beam, RF, and DC plasma discharges utilized hydrocarbon gases. Several applications of the films, including antireflection protective coat-

Correspondence concerning this article should be addressed to S. V. Babu.
Present address of M. David: 3M Company, St. Paul, MN 55101.

ings over infrared optical components and solar cells, protective barrier layers for plasma fusion reactors, magnetic and optical disks (Angus et al., 1989), low distortion coatings for high-frequency sound (tweeters), resist masks for nanometer lithography (Kakuchi et al., 1988), etc. have been investigated.

The versatility of the carbon films can be appreciated by describing their application in nanolithography as an example. It will also enable us to describe some of the desired properties of these films. In nanometer lithography, carbon films were utilized to yield patterns as small as 40 nm (Kakuchi et al., 1988) on thick silicon substrates. A dual-layer resist system comprising a film of a silicon-based negative resist (SNR) on top of a plasma-deposited carbon layer was used for patterning the substrate silicon. The carbon layer was deposited from an electron cyclotron resonance (ECR) plasma using acetylene and ethylene gases. The pattern created in the resist system was transferred to the underlying silicon using a fluorocarbon RIE process. The carbon film in the resist system had to have a low etching rate during the fluorocarbon RIE step for a faithful reproduction of the desired pattern in the silicon substrate. Properly deposited carbon films etched 2-3 times slower than conventional positive resists such as Microposit 1400 (a novolak-based photoresist demonstrating excellent RIE resistance) and PMMA (often used for nanometer patterning).

Carbon films were also used in nanolithography with other dual-layer resist systems consisting of positive e-beam resists such as poly (3-butenyltrimethylsilane sulfone) (PBTMSS) (Lin and Gozdz, 1988). PBTMSS was used as a top layer over diamond-like carbon. Both wet etching (in 10% iodic acid) and dry etching (in CH_4/H_2 plasmas) were used for transferring the pattern to InP and InGaAsP substrates. In both cases, DLC was an excellent bottom resist layer because of its superior structural integrity and chemical inertness.

Single-layer DLC resists, deposited from butane in an RF plasma and patterned by excimer laser projection lithography, were used directly over GaAs due to their excellent dry-etch resistance (Rothschild and Ehrlich, 1988). Linewidths as small as 0.13 μm were obtained by exposing the DLC films to 20 ns-ArF laser pulses, and the patterns were transferred to the substrate by dry etching. DLC resists displayed the best resolution among all resists in excimer laser projection lithography. Due to their low etch rates, smaller resist thicknesses can be tolerated, thereby increasing the resolution.

The carbon and DLC films used in nanolithography possessed a low etch rate, high selectivity, and superior structural integrity. The etch rate of a carbon film depends primarily on two factors, the hydrogen content and the extent of sp^3 bonding. The chemical composition and the degree of sp^3 bonding are influenced greatly by the deposition conditions.

The etching behavior of amorphous carbon can also give insights into the etching behavior of diamond, an important material for microelectronics. Sandhu and Chu (1989) postulated that the etching rate of diamond films is proportional to that of amorphous carbon films, the proportionality constant being roughly equal to the ratio of densities. They studied the oxygen etching of amorphous carbon films to understand the etching behavior of pure diamond. However, no attempt was made to correlate the etching rates with the deposition conditions.

The successful utilization of DLC films in all these applications was achieved by depositing conformal carbon films in a controlled fashion with the requisite etch rate and etch selectivity for the subsequent plasma-based pattern transfer process. Since amorphous carbon films exist in a whole spectrum of bonding configurations that depend on the deposition conditions, the etching behavior would vary significantly with the deposition conditions. Nevertheless, no systematic study of the relationship between the deposition conditions and the subsequent etch rate behavior has been reported. By elucidating and quantifying such a relationship, the potential of these carbon films in different applications will be realized more completely.

This article investigates this relationship in detail. Carbon films were deposited from the mixtures of butadiene, hydrogen and argon in an RF parallel-plate plasma reactor. The ion bombardment energy and the feed gas composition influence the extent of sp^3 bonding in the deposited film as well as its stoichiometry. For a fixed pressure, the substrate bias voltage and the C/H ratio of the feed gas are the interrelated quantities that control these two characteristics of the film. For a given C/H ratio in the feed gas, adding an argon diluent gas had a strong impact on the film properties. The deposited films were etched in O_2 and CF_4/O_2 plasmas. The etching behavior was correlated with the deposition environment by considering variations with V_b and the feed gas composition during deposition. A new nondimensional number provided an excellent generalized correlation for all the carbon films investigated.

Experimental Methods

A commercial parallel-plate plasma reactor (PlasmaTherm model 730/730) described earlier (David et al., 1990) was used for the deposition and etching experiments. The deposition chamber consists of a powered upper electrode and a grounded lower electrode. The chamber walls were also grounded. Single crystal silicon [100] and pyrex glass substrates were used as substrates for deposition and were stuck to the upper electrode by silver paint. The temperature of the upper electrode (0.28 m dia.) was maintained as 25°C by circulating ethylene glycol/water coolant mixture, while the temperature of the lower electrode was maintained at 400°C by a resistance heater. In the more conventional electrode configuration, substrates are placed on the lower, powered electrode and heated to the desired temperature (25–400°C). The reactor volume is 0.006 m^3, and the active discharge volume is 0.0025 m^3. Four outlet ports (0.04 m^3), arranged 90° apart on a 0.33-m-dia. circle on the lower wall of the reactor, lead the gases to a Roots blower backed by a mechanical pump. A capacitance manometer monitored the chamber pressure that was controlled by an exhaust valve and controller. The base pressure in the reactor was 0.13 Pa (1 mtorr), and the combined desorption and leak rate into the chamber was about 1.7×10^{-10} m^3/s (0.01 std. cm^3). A 600-W generator delivers RF power at 13.56 MHz through an automatic matching network to the reactor.

The etching chamber consists of similar-size electrodes (0.28 m dia.), with a coolant mixture circulated inside them to maintain a constant temperature of 25°C. The substrates to be etched were placed on the lower, powered electrode. The upper electrode and the chamber walls were grounded. The chamber shares the RF generator, vacuum plumbing, and gas supply systems with the deposition chamber.

Ternary mixtures of butadiene (99.99% pure; Matheson) or

(methane 99.999% pure; Linde), argon (99.999% pure; Linde), and hydrogen (99.99% pure; Linde) were used as reactant gases for deposition. The gases flow radially outward from a perforated electrode in a showerhead configuration in both of the chambers. This flow configuration differs from that utilized during the investigation of aluminum nitride deposition (David et al., 1990). The deposition experiments were carried out by maintaining the total flow rate and pressure fixed at 6.67×10^{-7} m^3/s (100 std. cm^3) and 7.2 Pa (55 mtorr), respectively. The 21 feed gas compositions selected for DLC deposition are shown in the ternary diagram (Figure 1). The stability of the plasma was influenced greatly by the feed gas composition and plasma power. Addition of argon stabilized the plasma at any given power level. All the films were deposited with 250 W of RF power, for which the plasma was stable over all the feed gas compositions.

Oxygen (99.99% pure; Linde) and carbontetrafluoride (99.999% pure; Linde)/oxygen mixtures were used for etching. Oxygen etching was carried out at a flow rate of 6.67×10^{-7} m^3/s (100 std. cm^3), a pressure of 13.3 Pa (100 mtorr), and a constant bias voltage of 230 V, with the substrates placed on the powered electrode. Films deposited with all the feed gas compositions shown in Figure 1 were investigated in the oxygen etching experiments. However, only the films deposited under the three-composition extremes in the ternary diagram (denoted by points A, B and C in Figure 1) were selected for etching in CF_4/O_2 gas mixtures at several different etch-gas compositions. CF_4/O_2 etching experiments were performed at a total gas flow rate of 5.34×10^{-7} m^3/s (80 std. cm^3) and a pressure of 13.3 Pa (100 mtorr) with the RF power fixed at 250 W. Film deposition and etching rates were measured by laser interferometry (Kleinknecht and Meier, 1978) using a He-Ne laser beam at near normal incidence. The reflected light was sensored by a photodetector. The output was connected to a chart recorder for measuring the oscillatory reflectance intensity produced by the changing film thickness. The rate of thickness change resulting from deposition or etching was calculated from the distance between adjacent peaks. The rate was obtained by averaging over 5 to 20 cycles.

Results

Growth environment

The pressure, the substrate bias voltage, and the nature and concentration of species present in the discharge are the important variables that determine the ion energy distribution and the film properties (Angus et al., 1986). At a fixed pressure, the average ion energy will increase with the bias voltage V_b, which depends on the feed gas composition and the power level. The ion energy distribution can change in different ways which depend on how the bias voltage is varied.

Since it was anticipated that the value of V_b has a strong influence on the properties and the etching characteristics of the deposited DLC films, the dependence of V_b on some of the deposition process parameters was investigated. The variation of V_b with the feed gas composition is shown in Figure 2. The data were obtained at a total pressure of 7.2 Pa (55 mtorr) and an RF power of 250 W. For a given percentage of argon, the bias voltage goes through a maximum, which is skewed toward hydrogen-rich mixtures. Addition of argon to a hydrogen-rich mixture reduced V_b, while the reverse occurred

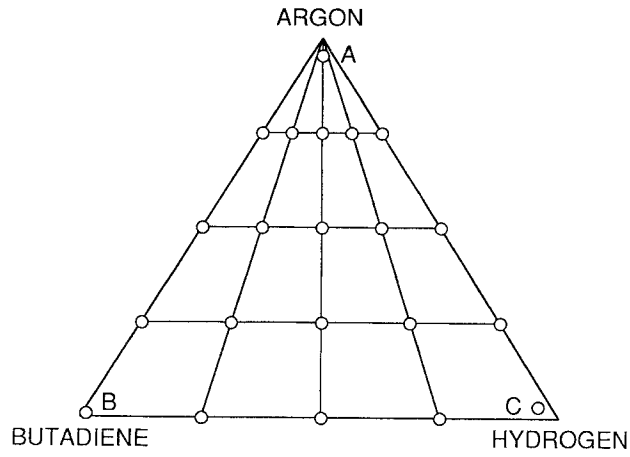

Figure 1. Ternary diagram showing the compositions selected for deposition experiments.

for hydrogen-deficient mixtures. The largest bias voltage of about 380 V occurred for an argon-free gas mixture containing about 20% butadiene, which corresponds to a feed gas C/H atomic ratio of 0.29. To determine whether higher bias voltages could be generated, the dependence of the bias voltage on the feed gas C/H ratio was investigated further at different power levels for argon-free mixtures, and compared with the results for methane/hydrogen gas mixtures. The results are shown in Figure 3. The bias voltage for a given power level has a broad maximum and has only a weak dependence on the C/H ratio. The bias voltage is essentially insensitive, in the range of overlapping C/H ratios to the identity of the hydrocarbon, with a maximum variation of only about 5%. The bias voltage, however, is a strong function of the plasma power.

Film deposition rates were measured for the various compositions shown in Figure 1. The variation of the deposition

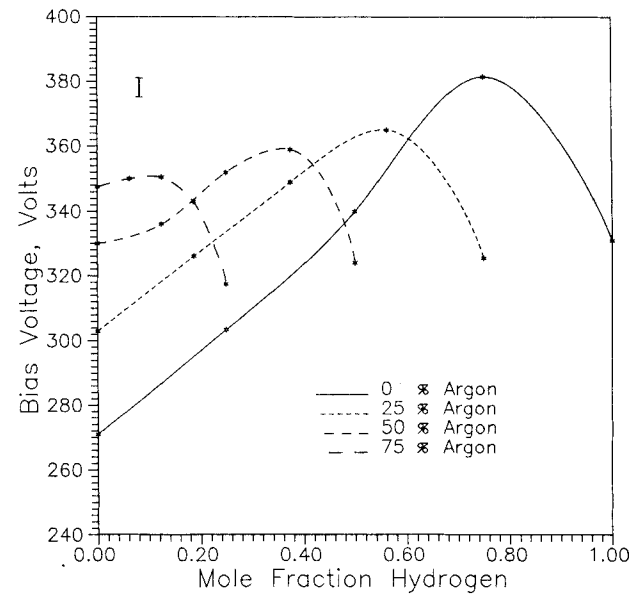

Figure 2. Bias voltage contours for the deposition of diamond-like carbon films.

The total gas flow rate, pressure, and plasma power were fixed at 6.67×10^{-7} m^3/s (100 std. cm^3), 7.2 Pa (55 mtorr), and 250 W.

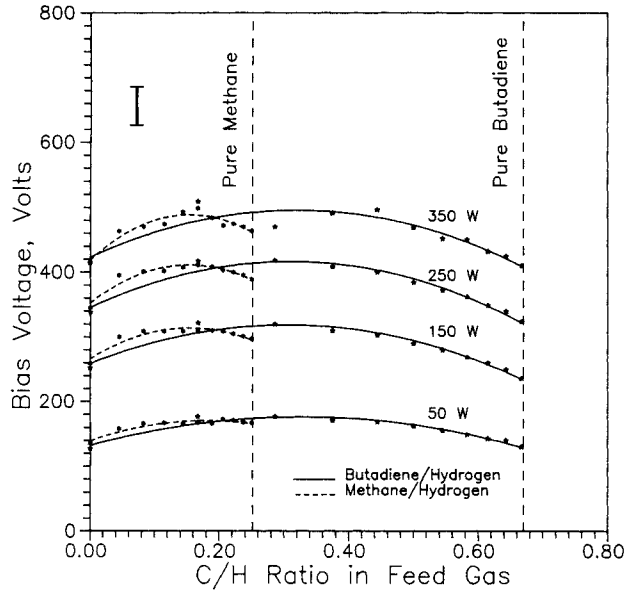

Figure 3. Variation of bias voltage with the feed gas C/H ratio for C_4H_6/H_2 and CH_4/H_2 mixtures.

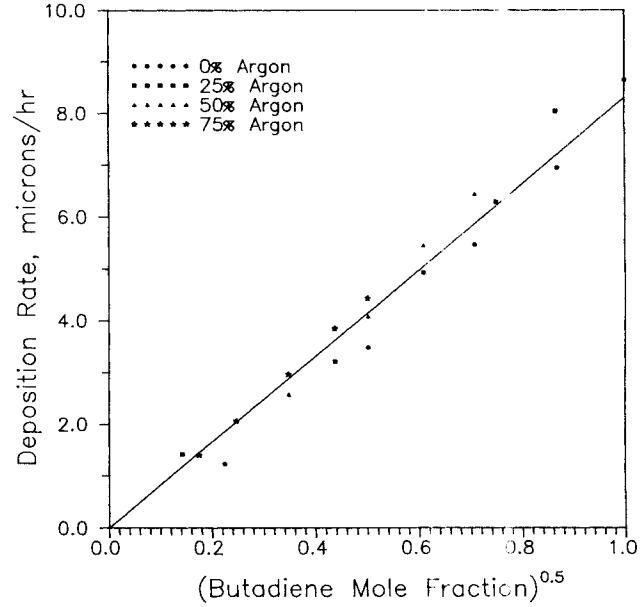

Figure 5. Variation of the deposition rate with butadiene mole fraction in the deposition feed gas mixture.

rate with the ternary feed gas composition is shown in Figure 4. The curves terminate at different hydrogen mole-fractions on the abscissa due to the varying percentages of argon. For example, the curve representing 75% argon terminates at a hydrogen mole fraction of 0.25 as the butadiene concentration approaches 0%. The deposition rates are relatively high, in the range of 1-9 μm/h and comparable to those of Bubenzer et al. (6 μm/h, using C_6H_6), Kobayashi et al. (0.2 μm/h, using CH_4) and Hoshino et al. (1 μm/h, using CH_4/H_2).

The deposition rate in our experiments is a strong function of the amount of argon and hydrogen present in the feed gas. The hydrocarbon species' concentration decreases with increasing amounts of hydrogen and argon, causing a monotonic reduction in the deposition rate. The deposition rate D varies as a square root of the butadiene concentration $[C_4H_6]$, as seen in Figure 5. The data fall on a single line, within experimental error, described by

$$D = (8.0 \pm 0.01)[C_4H_6]^{0.5 \pm 0.02} \quad (1)$$

The square-root dependence of the measured deposition rate on butadiene concentration suggests that the precursor molecules dissociate into two fragments in the gas phase and that these fragments diffuse and then react independently and individually on the growing film surface to form the DLC deposit. The square-root dependence also implies that the fragmentation step is not rate-controlling.

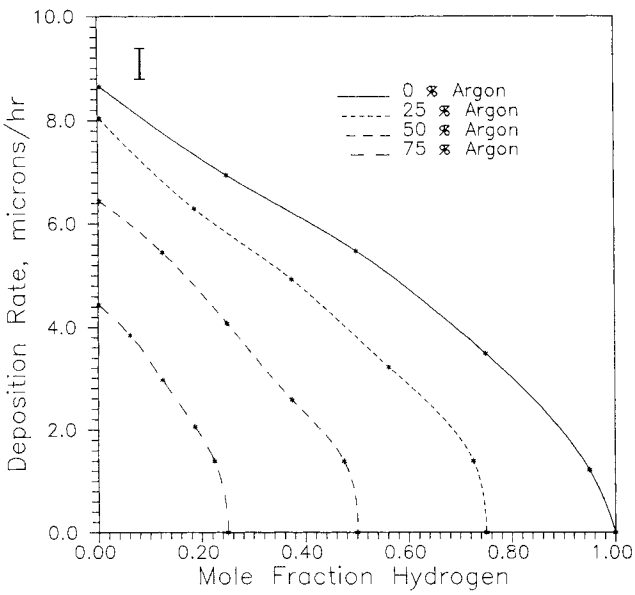

Figure 4. Deposition rate contours for diamond-like carbon films.

The total gas flow rate, pressure, and plasma power were fixed at 6.67×10^{-7} m^3/s (100 std. cm^3), 7.2 Pa (55 mtorr), and 250 W.

Film hardness and cracking

Films deposited in a hydrogen-rich atmosphere were soft and easily scratched, while films deposited at large C/H ratios were hard. In an argon-free gas mixture, even though the bias voltage varies only from 270 V to 330 V when the C/H ratio is changed from 0.67 to 0.0, large differences in hardness were observed. The hardest films were deposited in the argon-rich corner of the ternary diagram, when the C/H ratio is large. These films were difficult to scratch even with a silicon carbide scribing tool. However, as can be seen from Figure 4, it is very interesting to observe that precisely these films had the lowest deposition rates. There appears to be a trade-off between the rate of deposition and film hardness.

The difference in hardness may be related to a change from a diamond-like *hydro*carbon structure to a diamond-like carbon structure with increase in the feed gas C/H ratio. The feasibility of using the IR spectra of the films to characterize

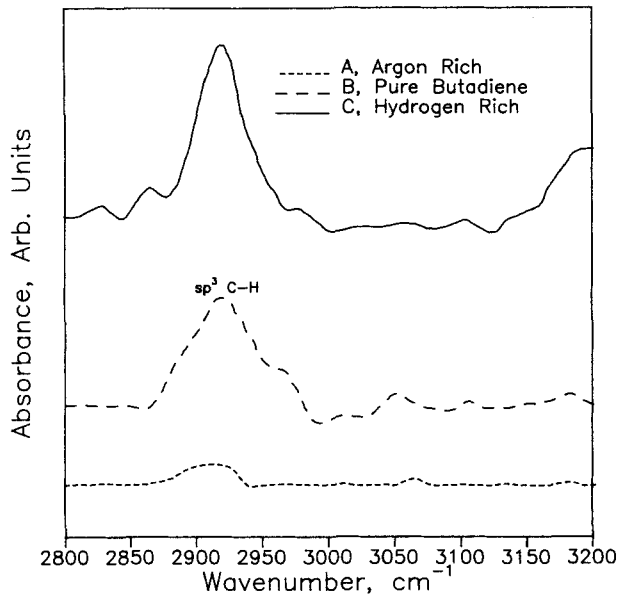

Figure 6. Infrared spectra of films deposited under compositions of A, B and C in Figure 1.

The films have an identical thickness of 900 nm.

this change was explored. The IR spectra obtained for the films deposited under the feed gas compositions labeled as A, B, and C in Figure 1 are shown in Figure 6. The films are about 900 nm thick. The absorption is highest at 2,920 cm^{-1} (sp^3 C-H stretching mode, Angus et al., 1984) for the three films. The total area under the CH_n absorption band is the highest for the film deposited with composition C and the lowest for the film deposited with composition A, in correspondence with decreasing hardness. However, the prominence of the sp^3 peak relative to the sp^2 and sp peaks in the three films implies that all the three films are *diamond-like*. Nevertheless, the change in hydrogen content and the change from a hard film to a soft film imply a transition from a diamond-like carbon film (sp^3 C-C bonds) to a diamond-like *hydro*carbon film (sp^3 C-H structure).

Film adhesion to silicon was far superior than to pyrex glass. Film cracking and peeling were noted for films thicker than about 3 μm over silicon and about 1 μm over glass. The failure

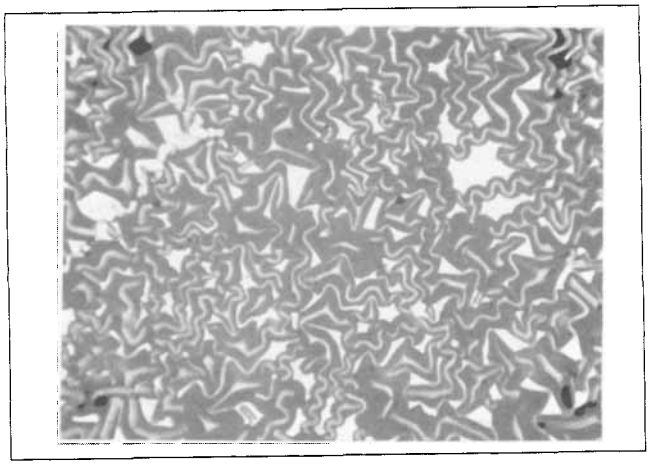

Figure 7. Optical micrograph showing film failure features over glass.

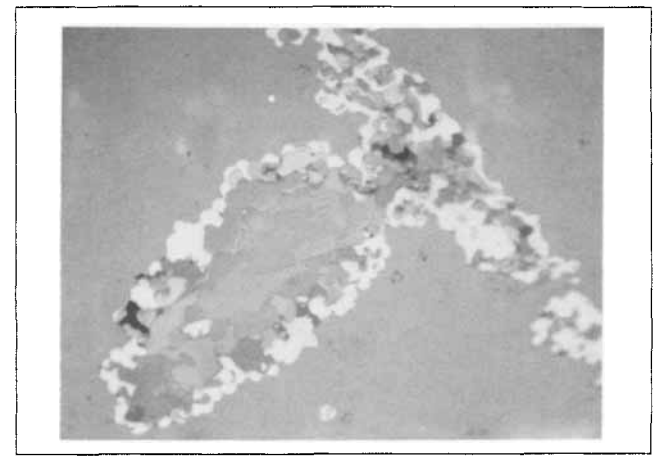

Figure 8. Optical micrograph showing film failure features over silicon.

mechanisms are substrate-specific, as seen from Figures 7, 8 and 9 for films grown in pure butadiene. Film buckling was observed over glass, originating near the edges of the substrate and propagating in winding paths (Figure 7) to the center. In contrast, no buckling was observed over silicon. However, flakes of carbon whose thickness is smaller than the total film thickness were delaminated (Figure 8). The failure clearly occurred within the film and not at the film-substrate interface. In an optical microscope, the different islands of film displayed different colors due to optical interference, indicating differing thicknesses. The color of any given island was uniform throughout its area, indicating that the films cracked as laminae. Moreover, broken flakes were seen over the other regions.

A rather dramatic failure mechanism was observed for films grown under argon-rich conditions. When the films were allowed to grow to several microns in thickness, numerous cracks were noted in films on the silicon substrates (Figure 9). These cracks were formed in the [100] and [010] directions of the single crystal silicon substrate. In extreme cases, enough stress was generated and the silicon substrates and the DLC film broke cleanly into multiple rectangular pieces that were a few millimeters wide on each side. These mechanical modes of failure of DLC films appear fascinating, but were not explored further.

Oxygen plasma etching

The pure-oxygen plasma etching rate data for all the films deposited with different feed gas compositions (see Figure 1) are shown in Figure 10 as a function of the mole fraction of hydrogen for different argon concentrations in the feed gas. As stated earlier, the films were etched with an oxygen flow rate of 6.67×10^{-7} m^3/s (100 std. cm^3), at a pressure of 13.3 Pa (100 mtorr) and a constant bias voltage of 230 V, with the substrates placed on the powered electrode. For a fixed argon concentration in the deposition feed mixture, an inverse proportionality between the etch rate and V_b may be noted. The etch rate goes through a minimum, approximately at the same location as the maximum in V_b (see Figure 3) for each of the curves.

With increasing argon content in the deposition feed gas, the etch rate drops gradually, the lowest etch rate occurring for films grown in an argon-rich environment. Again, these

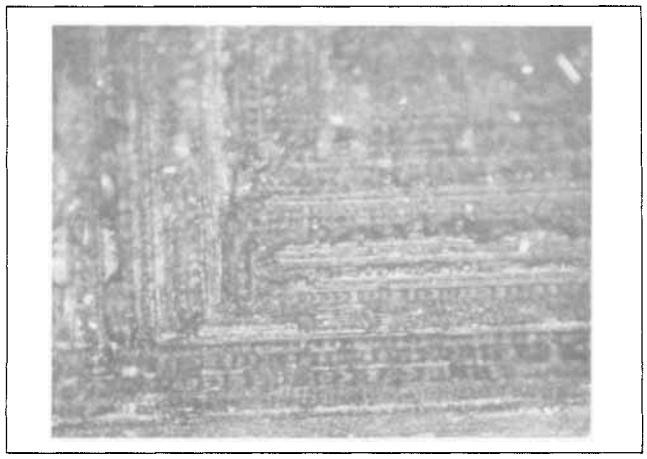

Figure 9. Optical micrograph of cracks formed over silicon substrate, with films grown under argon-rich conditions.

are the films with the lowest deposition rates and the highest hardness. However, the minimum in the etch rate is very broad and is not overly sensitive to the precise value of the butadiene-hydrogen ratio. For any given C/H ratio in the feed gas, addition of argon decreases the etch rate of the deposited film when the total flow rate is kept constant. Furthermore, the highest bias voltage which occurs at 0% argon, 20% butadiene, and 80% hydrogen, corresponding to a C/H ratio of 0.29 (see Figure 3) does not correspond to the smallest etch rate. This indicates that factors other than the ion bombardment energy are involved in determining the etch rate of the film. The smallest obtained etch rate is about 40 nm/min. In contrast, most polymer films show an etching rate exceeding 200 nm/min under similar etching conditions (Pederson, 1982).

CF_4/O_2 plasma etching

Only the films deposited under the conditions denoted by A, B, and C in Figure 1 were selected for measuring etch rates in CF_4/O_2 plasmas. The percentage of CF_4 in the gas mixture was varied from 0% to 100%. The results are shown in Figure 11 for the three films. As expected, all the three films showed negligible etch rate in pure CF_4. Oxides of carbon, which would form during oxygen etching, have a much higher vapor pressure than fluorocarbon species, which are formed in CF_4 plasmas.

Films deposited in an argon-rich environment (films A) display the smallest etch rate at all CF_4/O_2 compositions, in an apparent correspondence with their highest mechanical hardness as well as oxygen plasma etch rate. The etch rate profiles differ significantly from those for polymers, SiO_2, and SiC, which display a maximum in the etch rate for CF_4 concentrations ranging from 20% to 90%. The etch rate of films A and B is relatively constant at a low value for CF_4 concentrations between 70% and 100%. In contrast, Si and SiC have a maximum etch rate in that composition range. The etch rate of silicon carbide is maximum at a CF_4 concentration of around 80%. Depending on the crystallinity, the etch rate varies between 30 nm/min and 120 nm/min (Padiyath et al., 1991). Hence, excellent etch selectivities can be obtained using DLC films A and B over SiC films. However, such a potential use of DLC films as resist layers for patterning silicon carbide, a material of growing importance in the semiconductor industry, has not been explored yet.

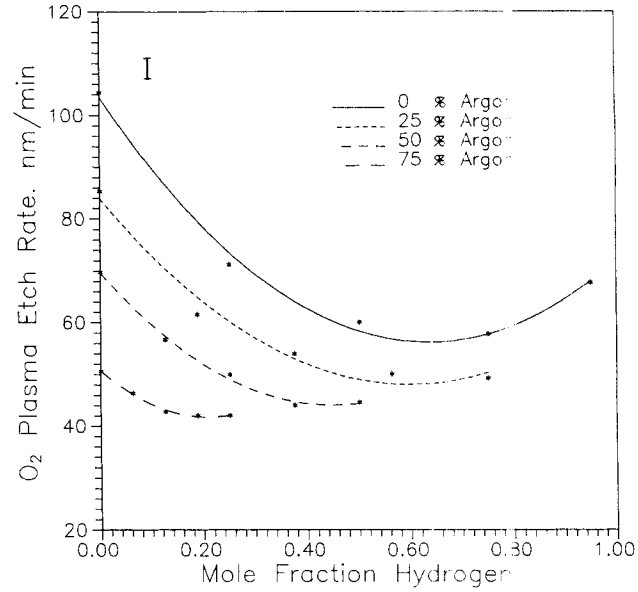

Figure 10. Etch rate of diamond-like carbon films in an oxygen plasma as a function of deposition feed gas composition.

The oxygen flow rate, pressure, and bias voltage during etching were fixed at 6.67×10^{-7} m^3/s (100 std. cm^3), 13.3 Pa, and 230 V.

Discussion

The nature and concentration of species present in the plasma discharge during growth depend on the discharge chemistry.

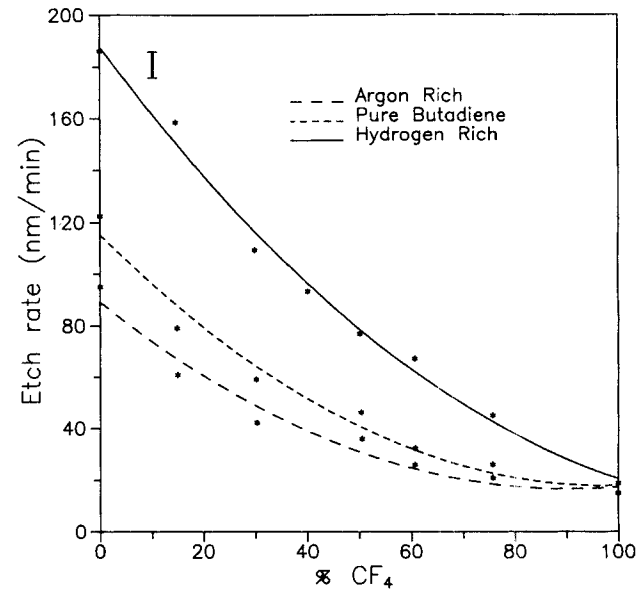

Figure 11. CF_4/O_2 etch rate of diamond-like carbon films deposited under compositions of A, B and C in Figure 1.

The total flow rate, pressure, and plasma power during etching were fixed at 5.34×10^{-7} m^3/s (80 std. cm^3), 13.3 Pa (100 mtorr), and 250 W.

The relative abundance of each of the species is altered significantly by changing the feed gas composition while keeping the pressure and the coupled plasma power constant. Plasma discharges of butadiene and hydrogen are unstable when the feed gas C/H ratio lies between 0.3 and 0.5. Addition of argon to these mixtures stabilizes the plasma. The bias voltage increases with plasma power and is relatively insensitive to the nature of the hydrocarbon (Figure 3). The deposition rate decreases with decreasing hydrocarbon concentration at any given argon concentration. The rate of decrease is higher at large concentrations of argon.

At small hydrocarbon concentrations, two different effects that lower the deposition rate are important. When the hydrogen concentration is large, chemical etching of the films during deposition is important. Carbon reacts with hydrogen to form volatile hydrocarbons which are pumped out in the exhaust. The deposition rate is therefore lowered. In the presence of excess argon, the deposition rate is lowered due to physical sputtering. In the absence of these two factors, (i.e., when the butadiene concentration is large), the deposition rate decreases with decreasing butadiene concentration due to a reduction in the hydrocarbon flux to the film surface.

The deposited film properties depend strongly on the relative amounts of sp^3 and sp^2-bonded structures present in it. The ratio of these structures in the film depends on their relative sputtering rates during deposition. Tetrahedrally coordinated sp^3 structures are assumed to be far more resistant to sputtering than trigonally-bonded sp^2 structures (Spencer et al., 1976). The displacement energies for carbon atoms in diamond (sp^3 C-C structures) and graphite (negligible sp^3 C-C structures) are 80 eV and 25 eV, respectively (Angus et al., 1986), well within the expected ion impact energies existing in RF discharges. Sputtering and deposition, therefore, occur simultaneously. Due to the greater sputtering efficiency of sp^2-bonded structures, the final deposit will be rich in sp^3 bonding if the deposition conditions favor sp^3 formation. The several desirable properties of diamond-like carbon films arise from the large fraction of sp^3 C-C bonding configurations present in them.

The sputtering rate during deposition depends on two factors: the ion impact energy and the ion flux to the substrate. It has been shown (Angus, 1986) that the film properties such as density, hydrogen content, refractive index, and optical absorption, depend on the ion impact energy during deposition. The mean ion impact energy I_E (eV/ion) is related to the bias voltage V_b and pressure P as follows (Angus, 1986):

$$I_E \propto V_b P^{-1/2} \tag{2}$$

The product of I_E (eV/ion) and the ion flux J_i (ions/cm^2·s) during deposition determines the energy flux to the growing film surface. The sputtering rate is directly proportional to the energy flux, and the preferential sputtering efficiency of sp^2-bonded structures is fixed for a given value of the energy flux. It is assumed here that at low deposition rates, sp^2 C-C and C-H structures are more likely to be excluded from the growing film due to their lower displacement energies and consequent higher sputter yields. The reverse situation occurs at high deposition rates. This implies that the ratio of the sp^3 to sp^2 bonding in the deposit would vary inversely with the deposition rate and is proportional to the energy flux. Therefore, we may write,

$$\frac{X_{sp^3}}{X_{sp^2}} \propto \frac{V_b P^{-1/2} J_i}{D} \tag{3}$$

where X_{sp^3} and X_{sp^2} are the fractions of sp^3 and sp^2-bonded structures in the deposit, and D is the deposition rate.

The etching rate of carbon films has been found to be inversely proportional to their density by Sandhu and Chu (1989). The density depends on the ratio of the amounts of sp^3 and sp^2-bonded structures present in the films (Angus et al., 1986), and it increases with the proportion of sp^3 structures in the films. Even though the DLC films have been etched in the RIE mode, the energy and ion fluxes during the etching process are not considered explicitly in the following discussion. Instead, the etch rate is assumed to be inversely proportional to the fraction of sp^3 and sp^2-bonding configurations in the film, Eq. 3. Hence,

$$E \propto \frac{D}{V_b P^{-1/2} J_i} \tag{4}$$

where E and D are the rates of etching and deposition, respectively. This relation is consistent with the results in Figures 4 and 10, where it can be seen that the etch rate is also related to the deposition rate. When the hydrogen concentration is fixed, increasing the argon concentration reduces both the deposition and the etch rates. The effects due to the substrate bias voltage (V_b) and the deposition rate (D) may be combined by taking these variables to the lefthand side of Eq. 4 to yield,

$$\frac{E \cdot V_b}{D} \propto \frac{1}{P^{-1/2} J_i} \tag{5}$$

The lefthand side may be nondimensionalized by dividing with kT_e/e where k is the Boltzman's constant, and T_e and e are the electron temperature and charge, respectively. The exact value of kT_e is unimportant, since it enters only as a scaling factor in Eq. 5 (Later on kT_e is taken to be 2 eV). Therefore,

$$E_N \equiv \frac{eEV_b}{kT_e D} \propto \frac{1}{P^{-1/2} J_i} \tag{6}$$

where E_N is a normalized etch rate that is nondimensional. The results presented later on provide a convincing *a posteriori* justification for the assumptions that were made in deriving this relation.

At constant pressure, the normalized etch rate E_N is inversely proportional to the ion flux J_i during deposition according to Eq. 6. The ion flux may be calculated from a detailed knowledge of the discharge chemistry. This would involve a discussion of the relative importance of processes such as electron impact dissociation, excitation, ionization, relaxation of electronically-excited atoms and molecules, recombination of ions and electrons, charge transfer reactions between ions and neutrals, ionization reactions due to metastable-neutral, metastable-metastable and metastable-electron collisions, etc. (Chapman, 1980, pp. 26–46). Furthermore, a knowledge of the concentrations and types of species present in the discharge as well as their collision cross-sections is required to model the plasma in detail.

A less detailed and simpler approach is proposed here. Ion-

ization is perhaps the most important process that determines the ion flux J_i. As an approximation, only electron impact ionization may be considered, since it is the primary process leading to ion production (Chapman, 1980, pp. 26–46). Assuming a Maxwell-Boltzmann distribution of electron energies (Chapman, 1980, p. 2) (more accurate, but complicated, electron energy distribution functions may be used for a more quantitative discussion), the ionization rate I per unit volume per unit time is given (Bell, 1974) as,

$$I = n_e n q \left(\frac{8}{\pi m_e}\right)^{1/2} (kT_e)^{1/2} \left(\frac{E_p}{kT_e} + 1\right) \exp\left(-\frac{E_p}{kT_e}\right) \quad (7)$$

where n_e and n are the number densities of electrons and neutrals undergoing ionization, respectively, m_e is the electron mass, q is the ionization cross-section, and E_p is the ionization potential. The ion flux J_i is directly proportional to the ionization rate. At constant pressure and plasma power, the number density n_e and temperature T_e of the electrons may be assumed to be approximately constant. After combining the various constants (n_e, T_e, q, k, m_e) of Eq. 7 into a proportionality factor, the ion flux J_i may be written as,

$$J_i \propto n(E_p + kT_e)\exp\left(-\frac{E_p}{kT_e}\right) \quad (8)$$

For ternary mixtures containing butadiene, hydrogen, and argon, ionization of each of the three species has to be considered separately due to their different ionization potentials and number densities. Therefore,

$$J_i \propto [C_4H_6](E_p^{C_4H_6} + kT_e)\exp\left(-\frac{E_p^{C_4H_6}}{kT_e}\right) + [H_2](E_p^{H_2} + kT_e)\exp\left(-\frac{E_p^{H_2}}{kT_e}\right) + [Ar](E_p^{Ar} + kT_e)\exp\left(-\frac{E_p^{Ar}}{kT_e}\right) \quad (9)$$

where the quantities in [ ] represent the number density of the corresponding species and E_p^j is the ionization potential of species j. The above equation may be simplified to yield,

$$J_i \propto [C_4H_6] + \left(\frac{E_p^{H_2} + kT_e}{E_p^{C_4H_6} + kT_e}\right)\exp\left(-\frac{E_p^{H_2} - E_p^{C_4H_6}}{kT_e}\right)[H_2] + \left(\frac{E_p^{Ar} + kT_e}{E_p^{C_4H_6} + kT_e}\right)\exp\left(-\frac{E_p^{Ar} - E_p^{C_4H_6}}{kT_e}\right)[Ar] \quad (10)$$

or

$$J_i \propto [C_4H_6] + C_0[H_2] + C_1[Ar]$$

where C_0 and C_1 are the constants that depend on the ionization potentials $E_p^{C_4H_6} = 9.07$ eV, $E_p^{H_2} = 15.427$ eV, $E_p^{Ar} = 15.759$ eV (*Handbook of Chemistry and Physics*, 1985, p. E-80), and the electron energy kT_e. The value of kT_e under typical discharge conditions is around 2 eV (Chapman, 1980, p. 51). Using these numbers, values of C_0 and C_1 were evaluated to be 0.0656 and 0.0566, respectively.

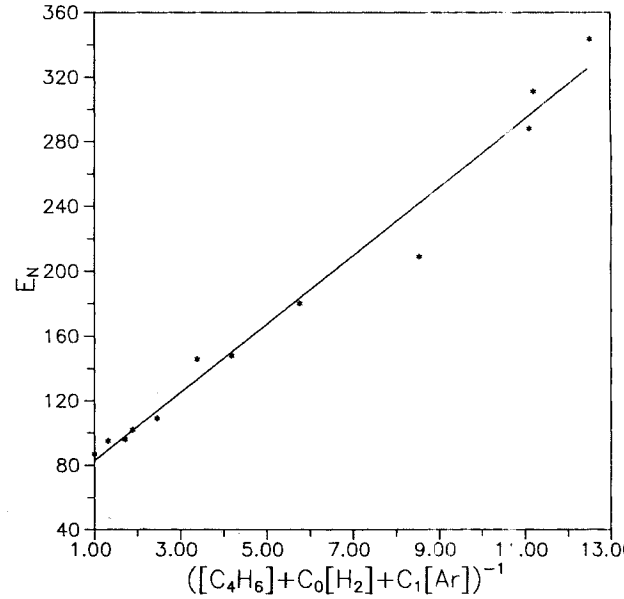

Figure 12. Variation of normalized oxygen etch rate (Eq. 11) with $([C_4H_6] + C_0[H_2] + C_1[Ar])^{-1}$.

Data from Figures 2, 4 and 10 were used for generating this plot. The linear relation validates Eq. 11.

By combining Eqs. 6 and 10, the normalized etch rate can be related to the feed gas composition. At constant pressure, E_N is inversely proportional to J_i, and hence,

$$E_N \propto \frac{1}{[C_4H_6] + 0.0656[H_2] + 0.0566[Ar]} \quad (11)$$

This is a relation that contains no adjustable constants other than the proportionality factor, and represents the etch rate and deposition rate data in a compact manner. The data required to test the validity of this equation for pure oxygen RIE etching of the films are available from the measurements obtained at a 130-W power level and reported in the earlier section. Thus, the etch rate (E), deposition rate (D), bias voltage (V_b), and feed gas composition ($[C_4H_6]$, $[H_2]$, [Ar]) data from Figures 3, 5 and 10 have been used to determine E_N as well as the righthand side of Eq. 11. The combined data are plotted in Figure 12, showing a linear relationship, within experimental error. There is more scatter at lower butadiene concentrations, since the righthand side of Eq. 11 becomes large. The equation of the straight line is:

$$E_N - E_{N,[C_4H_6]} = (22 \pm 2)[([C_4H_6] + 0.0656[H_2] + 0.0566[Ar])^{-1} - 1] \quad (12)$$

where $E_{N,[C_4H_6]} = 83 \pm 3$ is the normalized etch rate for films deposited in pure butadiene (righthand side of Eq. 11 is unity). It is concluded that the assumptions that led to the derivation of Eq. 11 are reasonable and that Eq. 11 provides a compact and consistent description of the combined deposition and etching data. It should be noted that all the etching and deposition rate data were obtained at a constant power of 130 W and 250 W, respectively. This correlation would be more com-

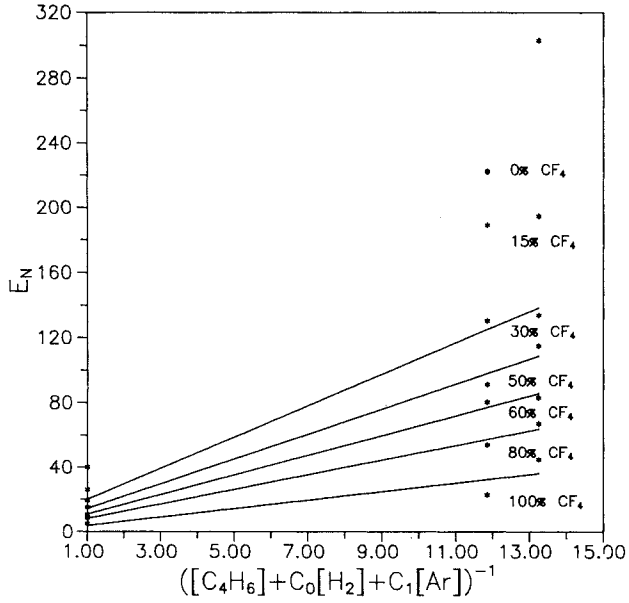

Figure 13. Variation of normalized CF_4/O_2 etch rate with $([C_4H_6]+C_0[H_2]+C_1[Ar])^{-1}$.

Data from Figure 11 were used for creating the plot.

pelling, if it can be shown that it represents etching and deposition data at other power levels also.

Furthermore, determination of the proportionality constant in this equation will enhance its utility for predictive purposes. This requires, among other things, the evaluation of the precise nature of the relation between the measured etch rate and the relative fraction of sp^3 configurations in the film. In particular, the dependence of the etch rate on the ion energy and ion flux under the RIE conditions in the O_2 and CF_4/O_2 discharges has not been considered explicitly in the above discussion. Also, the proportionality constant of Eq. 11 depends on the etching conditions, including power, pressure and flow rate, and on the etch gas composition. The composition dependence is illustrated by considering the etch rate in CF_4/O_2 plasmas. Three different data points (for films A, B and C) are available for each of the seven CF_4/O_2 compositions and are shown in Figure 13. A gradual change in the slope of the linear regression lines may be noted when the CF_4/O_2 composition is changed. Thus, the dependence of the proportionality constant in Eq. 11 on different process variables may be involved and its determination may require some adjustable parameters.

Conclusions

Diamond-like carbon films were deposited from ternary mixtures of butadiene, argon and hydrogen. Plasma stability was improved by adding argon. The IR spectra of the films deposited under three different composition extremes reveal sp^3 C-H bonds to be more prevalent than sp^2 C-H bonds. Films adhered better to silicon than to glass, and the failure mechanisms were substrate-specific. The hardness of the films ranged from easily scratchable to difficult-to-scratch with a silicon carbide scribing tool. The hardest films were deposited under an abundance of argon, and the softest films were deposited under an abundance of hydrogen.

The etching rate of the DLC films in oxygen and CF_4/O_2 plasmas is a strong function of the deposition conditions. The energy flux per depositing molecule determines the ratio of the sp^3 to sp^2 bonding in the deposited films. The etch rate, deposition rate and bias voltage were combined into a nondimensional number, E_N. A linear relationship between E_N and a function of the feed gas composition was derived (Eq. 11) by considering the generation of ions by electron impact ionization. The measured etch and deposition rate data, at 130 W and 250 W, respectively, are consistent with this relationship.

Acknowledgment

This research was supported by the Center for Advanced Materials Processing (CAMP) at Clarkson through a grant from the New York State Science and Technology Foundation and by an IBM fellowship to Moses David.

Notation

$[Ar]$ = mole fraction of argon
$[C_4H_6]$ = mole fraction of butadiene
$[H_2]$ = mole fraction of hydrogen
D = rate of deposition, nm/min
E = rate of etching, nm/min
E_N = normalized etch rate
E_p = ionization potential, eV
$E_p^{H_2}$ = ionization potential of hydrogen, eV
E_p^{Ar} = ionization potential of argon, eV
$E_p^{C_4H_6}$ = ionization potential of butadiene, eV
e = electron charge, C
I = ionization rate, ions/$m^3 \cdot s$
I_E = ion energy, J
J_i = ion flux, ions/$cm^2 \cdot s$
k = Boltzmann constant, eV/K
P = pressure, Pa
q = ionization cross-section
V_b = bias voltage, V
T_e = electron temperature, K

Literature Cited

Aisenberg, S., and R. Chabot, "Ion Beam Deposition of Thin Films of Diamond-Like Carbon," *J. Appl. Phys.*, **42**, 2953 (1971); *Thin Solid Films*, **40**, L31 (1977).

Angus, J. C., F. A. Buck, M. Sunkara, T. F. Groth, C. C. Hayman, and R. Gat, "Diamond Growth at Low Pressures," *MRS Bulletin*, **XIV**(10), 38 (1989).

Angus, J. C., and C. C. Hayman, "Low-Pressure Metastable Growth of Diamond and Diamond-Like Phases," *Sci*, **241**, 913 (1988).

Angus, J. C., P. Koidl, and S. Domitz, *Plasma Deposited Thin Films*, 89, J. Mort, and F. Jansen, eds., CRC Press, Boca Raton, FL (1986).

Angus, J. C., J. E. Stultz, P. J. Shiller, J. R. MacDonald, M. J. Mirtich, and S. Domitz, *Thin Solid Films*, **118**, 311 (1984).

Angus, J. C., H. A. Will, and W. S. Stanko, "Growth of Diamond Seed Crystals by Vapor Deposition," *J. Appl. Phys.*, **39**, 2915 (1968).

Bachmann, P. K., and R. Messier, *C & EN*, **4**, 24 (1989).

Bell, A. T., *Fundamentals of Plasma Chemistry*, Ch. 1, J. R. Hollahan and A. T. Bell, eds., Wiley, New York (1974).

Bubenzer, A., B. Dischler, G. Brandt, and P. Koidl, "RF Plasma Deposited Amorphous Hydrogenated Hard Carbon Films: Preparation, Properties and Applications," *J. Appl. Phys.*, **54**, 4590 (1983).

Chapman, B. N., *Glow Discharge Processes*, Wiley, New York (1980).

David, M., S. V. Babu, and D. H. Rasmussen, "RF Plasma Synthesis of Amorphous AlN Powder and Films," *AIChE J.*, **36**, 871 (1990).

Gautherin, G., and C. Weissmantel, "Some Trends in Preparing Film Structures by Ion Beam Methods," *Thin Solid Films*, **50**, L135 (1978).

Handbook of Chemistry and Physics, 66th ed., E-80, CRC Press, Boca Raton, FL (1985).

Holland, L., and S. M. Ojha, "Deposition of Hard and Insulating

Carbonaceous Films on an RF Target in a Butane Plasma," *Thin Solid Films*, **38**, L17 (1976).
Holland, L., and S. M. Ojha, "The Growth of Carbon Films with Random Atomic Structure from Ion Impact Damage in a Hydrocarbon Plasma," *Thin Solid Films*, **58**, 107 (1979).
Holland, L., and S. M. Ojha, "Infrared Transparent and Amorphous Carbon Grown under Ion Impact in a Butane Plasma," *Thin Solid Films*, **48**, L15 (1978).
Kakuchi, M., M. Hikita, and T. Tamamura, "Amorphous Carbon Films as Resist Masks with High Reactive Ion Etching Resistance for Nanometer Lithography," *Appl. Phys. Lett.*, **48**, 835 (1988).
Kleinknecht, H. P., and H. Meier, "Optical Monitoring of the Etching of SiO_2 and Si_3N_4 Films on Si," *J. Electrochem. Soc.*, **125**, 798 (1978).
Lin, P. S. D., and A. S. Gozdz, "High Throughput Nanolithography Using an Oxygen Plasma-Resistant Two-Layer System," *J. Vac. Sci. Technol.*, **B6**, 2290 (1988).
Martin, P. J., S. W. Filipczuk, R. P. Netterfield, J. S. Field, D. F. Whitnall, and D. R. McKenzie, "Structure and Hardness of Diamond-Like Carbon Films Prepared by Arc Evaporation," *J. Mat. Sci. Lett.*, **7**, 410 (1988).
Messier, R., A. R. Badzian, T. Badzian, K. E. Spear, P. Bachmann, and R. Roy, "From Diamond-Like Carbon to Diamond Films," *Thin Solid Films*, **153**, 1 (1987).
Ojha, S. M., and L. Holland, "Some Characteristics of Hard Carbonaceous Films," *Thin Solid Films*, **40**, L31 (1977).
Padiyath, R., R. Wright, M. I. Chaudhry, and S. V. Babu, "Reactive Ion Etching of Monocrystalline, Polycrystalline and Amorphous Silicon Carbide in CF_4/O_2 Mixtures," *App. Phys. Lett.*, **58** (Mar., 1991).
Pederson, L. A., "Structural Composition of Polymers Relative to Their Plasma Etch Characteristics," *J. Electrochem. Soc.*, **129**, 205 (1982).
Phillips, J. C., "Structure of Amorphous $(Ge,Si)_{1-x}Y_x$ Alloys," *Phys. Rev. Lett.*, **42**, 153 (1979).
Rothschild, M., and D. J. Ehrlich, "A Review of Excimer Laser Projection Lithography," *J. Vac. Sci. Technol.*, **B6**, 1 (1988).
Sandhu, G. S., and W. K. Chu, "Reactive Ion Etching of Diamond," *Appl. Phys. Lett.*, **55**, 437 (1989).
Spencer, E. G., P. H. Schmidt, D. C. Joy, and F. J. Sansalone, "Ion Beam Deposited Polycrystalline Diamond-Like Films," *Appl. Phys. Lett.*, **29**, 118 (1976).
Tsai, H., and D. B. Bogy, "Characterization of Diamond-Like Carbon Films and Their Application as Overcoats on Thin-Film Media for Magnetic Recording," *J. Vac. Sci. Technol.*, **A5**, 3287 (1987); Vora, H., and T. J. Moravec, "Structural Investigation of Thin Films of Diamond-Like Carbon," *J. Appl. Phys.*, **52**, 6151 (1981).
Weissmantel, C., "Film Preparation Using Plasma or Ion Activation," *Thin Solid Films*, **58**, 101 (1979).
Weissmantel, C., K. Bewilogua, and C. Schurer, "Characterization of Hard Carbon Films by Electron Energy Loss Spectrometry," *Thin Solid Films*, **61**, L1 (1979).
Weissmantel, C., C. Schurer, R. Frohlich, P. Grau, and H. Lehmann, "Mechanical Properties of Hard Carbon Films," *Thin Solid Films*, **61**, L5 (1979).
Weissmantel, C., K. Bewilogua, K. Breuer, D. Dietrich, U. Ebersbach, H. J. Erler, B. Rau, and G. Reisse, "Preparation and Properties of Hard *i*-C and *i*-BN Coatings," *Thin Solid Films*, **96**, 31 (1982).
Wada, N., P. J. Gaczi, and S. A. Solin, "Diamond-Like Three-Fold Coordinated Amorphous Carbon," *J. Non-Cryst. Solids*, **35**, 543 (1980).

Manuscript received Oct. 2, 1990, and revision received Jan. 3, 1991.